HHS Public Access

Author manuscript

Adv Mater. Author manuscript; available in PMC 2024 April 01.

Published in final edited form as:

Adv Mater. 2023 April ; 35(16): e2207882. doi:10.1002/adma.202207882.

Tunable Mesoscopic Collagen Island Architectures Modulate Stem Cell Behavior

Ryan Y. Nguyen[1], **Aidan T. Cabral**[1], **Alejandro Rossello-Martinez**[1], **Alessandro Zulli**[2], **Xiangyu Gong**[1], **Qiuting Zhang**[3], **Jing Yan**[3], **Michael Mak**[1,*]

[1]Department of Biomedical Engineering, Yale University, New Haven, CT, USA

[2]Department of Chemical and Environmental Engineering, Yale University, New Haven, CT, USA

[3]Department of Molecular, Cellular and Developmental Biology, Yale University, New Haven, CT, USA

Abstract

The ECM is the physical scaffold by which mammalian cells interact with their surrounding environment, of which the main constituent is collagen. In real tissue, collagen topology is diverse with complex mesoscopic features. While studies have explored the role of density and stiffness in collagen, the role of architecture remains largely unexplored. Thus, developing *in vitro* systems that recapitulate these diverse collagen architectures is critical for understanding physiologically relevant cell behavior. To this end, we developed a method to introduce heterogeneous architecture into collagen hydrogels, deemed collagen islands. These island gels have highly tunable inclusions and mechanical properties. Though these gels were globally soft, D1 mesenchymal stem cells (MSC) cultured in island gels can only deform the background fibers of these gels but not island inclusions themselves. We utilized these collagen island architectures to study MSC behavior and found that migratory and osteogenic differentiation capability were altered in island gels. Finally, we cultured induced pluripotent stem cells in our island gels and showed that architecture was sufficient to induce mesodermal differentiation. Overall, this work highlights complex tissue architecture as a bioactive cue in regulating cell behavior and presents a novel collagen-based hydrogel which captures these complex behaviors for tissue engineering applications.

Introduction

The extracellular matrix (ECM) is a highly complex structural scaffold that provides integral chemical and mechanical cues for cell growth and movement. The main constituent of

[*]**Contact Information for Corresponding Author:** Michael Mak, michael.mak@yale.edu.

Author contributions

R.Y.N. and M.M. designed the study. R.Y.N., A.T.C., A.R, and A.Z. conducted the experiments. R.Y.N., A.T.C., A.R., X.G., J.Y., and M.M. analyzed the results. Q.Z. helped with rheometry. A.R. carried out and analyzed the fluid dynamics simulations. A.R. developed the automated shear mixer. R.Y.N. and M.M. wrote the manuscript. All authors contributed to writing or editing the manuscript.

Code Availability

Algorithms were implemented in custom Python3 codes, and fluid dynamics simulations were implemented in COMSOL. All code is available from the corresponding author upon reasonable request.

Conflict of Interest Statement

The authors declare no potential conflicts of interests.

the ECM is collagen, the most abundant protein present in mammals. Collagen is able to act as a ligand for a diverse family of receptors, including integrins, receptor tyrosine kinases, and immunoglobulin-like receptors[1]. Altered ECM ligand concentrations and stiffness can also modulate intracellular signaling and cell differentiation [2–4]. In addition to its chemical properties, collagen can assemble into fibrillar network-like structures which display increased stiffness with increased density[5]. Studies have shown that stiff environments are important for a variety of cell behaviors such as migration, differentiation, and morphogenesis [6–10]. Stiffness of collagen fibers can also uniquely be modulated by force as they stiffen under increased strain [11,12]. Cells are able to take advantage of these complex mechanical properties and physically remodel the ECM to create stiffer environments [13–16] .

To study the role of the ECM on cell behavior, collagen hydrogels have been employed. Though the role of density and stiffness in bulk collagen gels has been extensively explored, these gels are often homogeneous and do not explore the role of mesoscopic architecture in cell behavior. To overcome this challenge, several studies have developed aligned collagen architectures by introducing a variety of factors - ranging from chemical modification to introducing flow-during collagen gelation [17–20]. However, collagen architecture in the body comes in other diverse forms.

In real tissue, the landscape of the ECM can be varied with locally sparse regions, where cells are able to move, interspersed with locally dense regions. This variable ECM landscape subsequently results in heterogeneous spatial distribution of ECM proteins such as collagen as well as nonuniform tissue stiffness. It has also been shown that altering the spacing of ligands on 2D polyacrylamide can drastically increase cell spreading and behavior even on soft substrates[21]. In addition, studies have characterized collagen architecture as a key regulator of cell behavior by affecting nutrient availability as well as migration capability [22,23]. However, collagen gels used in these studies all have relatively uniform architectures and do not capture spatial heterogeneity seen *in vivo*. Thus, developing *in vitro* systems that recapitulate these diverse ECM architectures is critical for understanding physiologically relevant cell behavior. However, tuning conventional parameters for collagen gelation, such as temperature, pH, and ion concentration, only results in limited architectural tunability. In the field of tissue engineering, it is therefore crucial to faithfully mimic tissue architecture to better program cell behavior in tissue assembly.

To address this need, we have developed a method for creating fully collagen I based hydrogels with heterogeneous inclusions, deemed collagen islands. Collagen island size can be easily fabricated and varied by modulating rates of mechanical fragmentation. In addition, these gels have tunable bulk mechanical properties that can be advantageous for studying a range of cellular functions. The tunability in local architecture in these island gels is able to give rise to a variety of stem cell differentiation behaviors. The programmable and modular nature of these gels makes them suitable scaffolds for microtissue fabrication in physiologically relevant environments. Overall, these highly tunable gels have the potential to be used in a variety of tissue engineering applications.

Results

Figure 1: Introduction of collagen architecture and collagen island architecture

In physiological tissues, ECM topologies and architectures can be diverse, with regions of varying density and stiffnesses (Fig 1a). These properties are crucial for determining cell function. To recreate the heterogeneous architecture of physiological ECM, we developed a method to introduce inclusions into collagen hydrogels. This process involved mechanical fragmentation during the collagen gelation process at regular intervals to produce collagen "island" inclusions embedded into the hydrogel. By modulating shearing frequency, the amount of shear stress introduced during gelation was altered (Fig 1b).

Fluid dynamics simulations revealed how much shear stress and energy are introduced into our gels during this process (Fig S1a, Video S1). By shearing at a higher frequency, we found that more energy and shear stress were introduced into our system (Fig S1b). Interestingly, while most of the shear stress being introduced into the system comes from shear induced by the pipette tip, a significant amount of stress developed as the fluid hit the bottom of the centrifuge tube. These simulations allowed us to separate island gels into distinct architectures based on the shear frequency: a high shear island gel (oscillatory mixing with a period of 2 seconds), a mid shear island gel (oscillatory mixing with a period of 5 seconds) and low shear island gel (oscillatory mixing with a period of 10 seconds). We hypothesized that increasing the amount of shear stress introduced into the gel would break apart these islands into smaller fragments.

In accordance with our simulations, we found that island size could be reproducibly modulated with high shear island gels having smaller islands and low shear island gels having larger islands (Fig 1c). During the mixing stage, collagen gelation has not completed as this is occurring during the transient gelation phase right after collagen neutralization. Thus, nucleation, polymerization, gelation, and agglomeration are all occurring during island gel synthesis. Large scale confocal microscopy and subsequent 3D reconstructions reveal that these island architectures are well distributed throughout the gel (Fig S3). All gels are a final concentration of 2 mg/ml. For simplicity, isotropic 2mg/ml gels with no mechanical perturbation are referred to as normal gels. These island architectures and their packing within the gel were observable at the macro, meso and nano scales. Confocal microscopy revealed that increasing shearing frequency caused inhomogeneity in pore size in our gels, indicated by higher occurrence of larger pore areas (Fig 1d, right side of dotted line). This suggested that, as shear frequency increases, more collagen became a part of the island architecture and the background fibers became more sparse. Furthermore, confocal microscopy revealed that mechanical shearing introduced inhomogenous architectures into the collagen gel and that increasing shearing frequency decreased the packing fraction of islands (Fig 1e, Fig S4). These islands are highly stable, being able to be spun down and resuspended in smaller volumes of collagen or in different biomaterials to tune island packing fraction (Fig S5). Increasing mechanical fragmentation yielded hydrogels with smaller islands as well as softer bulk stiffness as determined by shear rheometry (Fig 1f–g). While bulk stiffness is used here, confocal microscopy suggested local differences in stiffness in island gels, with the islands being higher density collagen structures and,

therefore stiffer than the background collagen embedded between the islands[5]. In order to improve scalability, we further developed an automated collagen mixer (Fig S6a–b). We were able to input shear frequencies and recapitulated collagen island architectures made by hand (Fig S6c). Future studies can further utilize this tool to scale up and automate island architecture assembly as well as efficiently explore the phase space that underlies island architecture. Together, these data suggested that collagen islands are easily tunable with the capability for modular assembly.

Figure 2: Mechanical properties of tunable collagen islands

Stiffness is only one mechanical property of biomaterials that can affect cell behavior. In particular, collagen can undergo nonlinear strain stiffening in which collagen can increase in stiffness significantly under increasing applied strain. Notably, cells are able to mechanically remodel collagen to sufficiently induce strain stiffening, creating stiffness gradients over hundreds of microns [24–26]. Strain stiffening has been shown to contribute to a variety of cell behaviors including durotaxis, focal adhesion development, and higher migratory behavior. In addition, collagen is viscoelastic and can reorganize molecularly over time under applied strain leading to stress relaxation. Viscoelasticity in biomaterials has been implicated in a number of cellular processes including cell spreading, cell migration, and differentiation [27–30]. While these properties have been studied extensively in the literature, how tissue architecture affects these mechanical properties is poorly understood.

Given the distinct architectural organization of collagen islands, we next interrogated the bulk mechanical properties of these gels. Rheological shear strain sweeps revealed that all collagen island architectures maintained their strain stiffening capabilities (Fig 2a). Onset of strain stiffening occurred in all gels between 12-16% strain. We defined a differential shear modulus K to describe bulk stiffness as a function of strain (physical description in Fig S7). We found that high shear island gels were significantly softer than an isotropic collagen gel. In addition, high shear island gels reached a smaller plateau K and failed under lower strains (Fig 2b, Fig S8). This could be due to increased mechanical fragmentation introduced during gelation which resulted in less dense background fibers that strain-stiffen and fail under lower shear strain.

We next performed stress relaxation tests at different strains to determine the viscoelastic properties of our island gels. We found that all gels exhibit strain dependent stress relaxation properties, in which higher strains lead to faster stress relaxation (Fig 2b, Fig S9). This behavior in isotropic collagen gels has been reported previously[31]. We found no observable differences in normalized viscoelastic behavior between island gels at any strain (Fig 2c, Fig S10). values were approximately 10, 5, and 3 seconds for all gels at 10%, 30%, and 60% strain, respectively. We found that max stress values increased with increasing strain, which was in accordance with our strain sweep data (Fig S11). This data suggested that the ability of collagen fibers to relax under applied strain was unaffected by mechanical fragmentation. Together, these results suggested that our island gels maintain both the ability to strain-stiffen and stress relax. Unlike normal collagen gels in which these properties have to be tuned by changing either the density of collagen gels or by adding molecular

crosslinkers[32], collagen island gels have tunable bulk mechanical properties without these alterations.

Figure 3: Cell contractile behavior is modulated by heterogeneous architecture

After determining the bulk mechanical characteristics of our gels, we next explored how these differences in architectures could affect collective cell-matrix interactions. To this end, we performed gel compaction assays in which we embed D1 murine mesenchymal stem cells (MSCs) in gels and monitor gel area over time (Fig 3a). Understanding MSC behavior in these gels are of particular importance for their use in tissue engineering. To initially understand cell behavior in our gels, we performed gel compaction assays in which 15 μl gels of different architectures are plated on microwell plates and imaged over 12 hours (Fig 3b–c, Video S2–4). These plates were coated with 3% BSA to prevent collagen sticking to the plate. Over the course of the timelapse, we observed densification and alignment profiles in the isotropic normal gels (Fig 3c, white arrows). Such profiles are indicative of local strain stiffening in the network[11,33]. Conversely, cells were unable to deform collagen islands likely because they are too stiff to be mechanically remodeled. While all island gels showed very little plastic tracks, they do show densification of islands indicated by their compaction (Fig 3c, yellow arrows). This suggested that cells were more able to remodel the normal (thin) collagen fiber network and the thin background fiber network which percolate between the islands than the islands themselves.

When we further examined cell-matrix interactions in the normal or mid shear island gels, we noticed differences in dynamic protrusion activity. We found that MSCs were highly dynamic in normal gels and demonstrated the ability to form many long protrusions and densify collagen around themselves (Fig 3di). However, MSCs cultured in island gels formed smaller protrusions and showed less densification of surrounding collagen. In addition, MSCs cultured in these gels could send out protrusions and cause movement of neighboring mesoscale islands (Fig 3dii, yellow arrow). We also note that once these protrusions retracted, the islands were able to recoil back near their original position, suggesting elastic deformations at this timescale (Fig 3dii, white dotted lines). Together, these data suggest that MSCs cultured in island gels have fewer dynamic protrusions and, therefore, are less able to initially non-elastically densify their local surroundings via nonelastic recruitment through protrusions [13]. This may be due to fewer available thin fibers in the background of island gels for protrusions to be generated onto and to recruit. This may also be due to the background network being softer (due to reduced collagen concentration), thus reducing cell contractility via mechanosensing[34,35].

We next performed standard gel compaction assays and monitored compaction over the course of 7 days (Fig 3e). Wells were again coated 3% BSA to prevent the collagen from sticking to the plate. We found that the high shear island gels compacted significantly quicker than did the isotropic gel on days 2 and 3 but also eventually converged to the isotropic gel compaction area (Fig 3f–g). This was in agreement with our rheometry data which showed that high shear island gels are softer and can be strain stiffened at lower strains. Interestingly, we found that mid shear and low shear island gels compacted significantly slower than isotropic 2mg/ml gels over the course of the first 3 days but then

eventually converged to the isotropic gel compaction area with the mid shear island gels compacting the slowest. Immunofluorescence of cells after 2 days of culture in compacting gels revealed no significant difference in cell morphology or cell proliferation (Fig S12). To compare, we also monitored gel compaction of a 4mg/ml collagen gel which compacted significantly slower than all island and normal gels and also compacted to a higher plateau area (Fig S13a).

In addition to elastic deformation of fibers within the gel, cells dynamically remodel the matrix and plastically deform the gel [13]. Plastic deformation of fibers within gels can play a major role in gel mechanics which will in turn give rise to altered cellular response. To determine the amount of plastic deformation, we removed/lysed all cells with SDS after 7 days of culture. We observed a 1-3% increase in gel area, indicating that the majority of gel compaction was nonelastic (irreversible).

Given that MSCs cultured in our mid and low shear island gels compacted less quickly than those cultured in normal gels and that MSCs cultured in island gels showed less dynamic protrusions, we sought to rescue gel compaction by increasing dynamic protrusion activity. Thus, we incubated MSCs cultured in mid or low shear gels with agonists for either RhoA or all RhoGTPases. These particular molecular targets are known to affect cytoskeletal dynamics and are key players in collagen remodeling[36,37]. We found that treatment with RhoGTPase agonist was sufficient to increase gel compaction rate in mid and low shear gels to that of normal gels (Fig 3g, Fig S13b). Future dosing studies will further help dissect the individual role of different RhoGTPases and cytoskeletal factors in gel compaction in these environments. Together, these data suggest that our collagen island architectures can modulate compaction behavior of cells and that this can be further modulated by altering RhoGTPase activity.

Figure 4: Island architecture modulates MSC cell behavior

To determine how island architecture modulates stem cell behavior, we next seeded D1 MSC's in gels that were adherent to polydopamine covered glass (Fig S14). Polydopamine allows for collagen to remain anchored to surfaces for imaging and prevents total compaction of the gel during experiments [38]. We then visualized MSC migration in our gels. To capture cell migration in these gels, we generated a stably transduced LifeAct-RFP dye into our MSCs and then imaged these encapsulated cells with time-lapse confocal fluorescence microscopy. We then performed cell tracking analysis to determine migration metrics (Fig 4a). We imaged the cells both 1 day after seeding and 6 days after seeding for 12 hour timelapses. After 1 day of culture, we observed higher mean speeds in all island gels compared to normal gels but no differences in migration track length (Fig S15a–b). After 6 days of culture, we observed differences in migratory behavior between MSCs cultured in different island gels (Fig 4b). Timelapses of our data indicated that MSCs tended to migrate around the islands and moved through the background fibers and did not move through islands (Video S5–8). We find that MSC migration speed was slow in both the normal and high shear island gels, increases in mid shear island gels, and then decreased again in low shear island gels. This bell curve was observed in mean sphericity of cells and migration track length. As a control, we treated our cells with inhibitors of myosin-based

contractility (NSC23766 for Rac1, ML-7 for myosin light chain kinase, and Y-27632 for Rho-associated kinase (ROCK)), and saw decreases in cell migration track length for all conditions (Fig S16a). Together, these data suggested that migratory capability in these gels could be modulated by the ratio of background fibers to islands and that there is an optimal island architecture to promote migration.

To further investigate how these gels affected MSC behavior, we next looked at MSC osteogenic differentiation after 7 days of culture. Previous studies have shown that substrate stiffness can affect differentiation capability, with softer substrates showing less osteogenic commitment [10]. As a control to verify these results, we encapsulated our MSCs on collagen gels of increasing density and, therefore, increasing stiffness. Indeed, we saw increased osteogenic commitment of cells in increasing collagen density (Fig S17). Given these results and our stiffness measurements, we initially hypothesized that there would be less differentiation in island gels. Interestingly, osteogenic commitment of these MSC's also follows a bell-shaped curve (Fig 4b). ALP signal was low in normal and high shear island gels, increased significantly in mid shear island gels, and then decreased in low shear island gels (Fig 4d). Differences in cell division are not detectable between island conditions (Fig S16b). We further confirmed osteogenic commitment by staining for calcium deposition with Alizarin red (Fig S16c). Since our cells were cultured in 50/50 osteogenic and adipogenic induction media, we also stained for adipogenic commitment but did not see significant adipogenic activity (Fig S16c). Pharmacological inhibition of myosin-based contractility caused a decrease in ALP positive staining (Fig S16d–e).

To further investigate this differentiation behavior, we analyzed localization of RUNX2, a key transcription factor in osteogenesis [39,40]. We again found a bell-shaped curve in RUNX2 nuclear localization with the highest amount of nuclear RUNX2 found in the mid shear gels (Fig 4e–f). Pharmacological inhibition of myosin-based contractility also inhibited RUNX2 nuclear localization (Fig S16f). Interestingly, treatment of MSCs with either RhoA or RhoGTPase agonist actually decreased osteogenic commitment and promoted cellular network formation (Fig S16g–h, Fig S18). Cells are able to spread in all conditions, and there is heterogeneity in how much they spread (Fig S16g). Their shapes can change dynamically over time (Videos S5–S8). We note that interestingly, even though cells can spread in all conditions, there is a bell shaped curve in osteogenic commitment versus island architectures.

Our results, which reveal a bell-shaped curve in osteogenic commitment in island architectures, could be explained by the complex architectures of these island gels. Though the bulk stiffness of these gels is soft, the islands provide high local stiffness which modulates stem cell behavior. Our data suggest an optimal spacing of stiff inclusions to promote cell spreading. Our results indicate an optimal island architecture for osteogenic differentiation which cannot be achieved in normal isotropic collagen gels.

Figure 5: iPSCs undergo differentiation in island architecture

Given that our results showed that the mid shear island gels provided optimal cell behavior in terms of spreading and differentiation, we next investigated how this architecture could affect iPSC behavior. We encapsulated single cell iPSC suspensions in either normal

or island gels and varied the amount of matrigel concentration. We cultured iPSCs in conditions in which matrigel made up either 20% or 50% of the final volume, and PBS was added to the 20% matrigel solutions to create equal volume solutions. In both cases, normal gels or island gels made up 50% of the final volume. We then monitored growth of our iPSCs over the course of 7 days without the addition of differentiation factors (Fig 5a). Our island architectures are fabricated before being added into matrigel. This eliminates the possibility of changes in collagen island gelation kinetics as the islands are already formed. As shown in previous studies [41,42], iPSCs grown in pure Matrigel self organized to form lumen-like structures and maintained their pluripotency after 7 days of culture(Fig S19a). While cells grown in 20% matrigel solutions tended to form circular lumens, those grown in 50% matrigel solutions started showing invasive strands. Measurements of solidity and circularity showed that this phenotype appears after 3 days of culture and continued to diverge from the 20% conditions further over the course of the experiments (Fig 5b, Fig S20). Notably, roughly 30% of the iPSC lumens grown in 50% matrigel gels showed these invasive phenotypes whereas almost all of the iPSC lumens grown in 50% island gels showed invasive strands, suggesting that the islands helped push the iPSCs to a differentiated state (Fig 5c).

We next sought to understand how island architecture could affect stem cell fate. We looked at the canonical markers for pluripotency, ZO-1 and Nanog [41]. Immunofluorescence staining of these structures revealed that cells cultured in 50% island gels lose both their stemness as well as their apical basal polarity, indicated by a loss of Nanog and ZO-1, respectively (Fig 5d). Further confirmation of pluripotency loss was shown by a lack of SOX2 expression in 50% island gels. We next stained our cells for the canonical mesodermal markers Snail and Brachyury [41,43]. After 7 days of culture, we found that cells cultured in 50% island gels show nuclear localization of both Snail and Brachyury, indicating mesodermal differentiation (Fig 5e–f). We further confirmed mesodermal differentiation via qPCR and saw a significant decrease in expression of NANOG and SOX2 (pluripotency markers) and a sharp significant increase in TBX6 (mesodermal markers) (Fig S21). We saw no significant differences in expression of either ectoderm (OTX2) or endoderm (SOX17) markers. We also found expression of vimentin, a canonical EMT marker, in invasive cells cultured in 50% normal gels and in all cells cultured in 50% island gels (Fig S19B). The mechanism behind this differentiation pattern must be further explored. This phenomenon could be explained by a number of gel properties such as asymmetric distribution of ligands as well as heterogeneous local stiffnesses. Together, these data suggest that architectural cues, and notably islands, are sufficient to induce mesodermal differentiation of iPSCs. Overall, these island architectures may prove to be a useful tool to induce differentiation.

Discussions

Heterogeneity in ECM architecture is present in all tissue types. This varied tissue topography results in differences in pore size, stiffness, and ligand concentration and, subsequently will give rise to a spread in cell behavior. Developing *in vitro* systems which recapitulate this heterogeneity is, therefore, crucial in understanding how local architectural cues can influence bulk tissue behavior for tissue engineering. Here, we developed collagen island gels which accurately depict features found in many real tissues. Island gels are

relatively simple to manufacture as they only require mechanical shear to form and also have tunable island size depending on mechanical shear frequency. Furthermore, these islands are able to be isolated from solution and resuspended in other natural ECM-derived matrices. Altogether, these island gels mimic tissue architecture, have tunable topographical and mechanical properties, and are compatible with modular assembly for tissue engineering.

Our fluid dynamics model was able to obtain metrics of shear stress and energy introduced into the system. While we note that this model does not take into account key metrics such as gelation, it could give us some predictive power in terms of defining the full phase space of collagen islands. The model allows us to predict how changes in pipetting frequency, pipette geometry, and even distance of pipette from bottom of the tube could affect total energy output and, therefore, island architecture. Further studies will address how changes in these parameters will affect overall spacing and size of islands. Characterizing the phase space of these island gels will help guide optimal recipes for the assembly of mesoscopic ECM architectures and uncover key mechanical driving factors. This will allow for the study of physiologically mimicking heterogeneous and mesoscopic cues, which typical hydrogel gels do not offer but are important physiologically and pathologically [44,45].

Much of the literature has shown that global stiffness is able to modulate differentiation behavior [10,46,47]. However, bulk stiffness values are measured at a scale much larger than what cells are able to sense. In addition, local stiffness profiles do not necessarily correlate with global stiffness. Thus, local stiffnesses may be more crucial in determining cell fate. Our island gels, though globally soft, have locally stiff inclusions and are still able to induce early osteogenic commitment in MSCs. This is likely due to the islands acting as locally stiff inclusions which the cells are able to sense and interact with. However, stiffness alone is not sufficient to induce MSC differentiation as MSCs cultured in low shear islands show lower osteogenic differentiation as well as less migration. Low shear islands are more packed and have less empty space between islands to promote cell spreading in those empty spaces which may cause cell confinement. The interplay between island spacing and island stiffness could be a key factor in modulating cell behavior. Given that island concentration can be tuned simply by centrifugation, future studies will look into how varying the packing fraction of these islands could affect cell fate.

Bulk mechanical properties of these island gels are tunable. Their bulk stiffness is able to be modulated. However, AFM is still required to probe the local mechanical properties of these island architectures. In addition, while viscoelasticity has been shown to be a determinant of cell behavior in 3D hydrogels, bulk normalized viscoelasticity does not seem to be affected by introduction of island architecture. However, this constant viscoelastic behavior remains poorly understood. We hypothesize that, while the network of the collagen has experienced significant rearrangement, longer fibers (which are the main contributors of viscoelasticity) remain unaffected. A particularly useful tool for teasing apart these mechanics are discrete fiber network models, which have been used extensively to understand local network behavior of various biomaterials under applied stresses [48,49]. Future studies will incorporate these models to better understand the mechanical contributions of these islands to bulk properties. Overall, our data suggests that local stiffness, island spacing, and connections between islands are all important cues that affect cell behaviors in our gels.

Typically, differentiation of iPSCs requires specific addition of chemical signals. It has previously been shown that asymmetric distribution of chemical signals is sufficient to drive mesodermal transitions of stem cells in 3D culture[50]. Our island gels were able to direct spontaneous iPSC differentiation. We observed that our iPSCs cultured in island Matrigel co-gels started this transition after 3 days in culture and will nuclearly express markers of mesodermal commitment. These results suggested that architecture may be sufficient to drive differentiation. We note that addition of matrigel would affect bulk mechanical properties of collagen island gels and could affect cell behavior. However, the molecular mechanism behind this remains unexplored. Studies have implicated BMP4 as a key determinant of the mesodermal transition [41,50,51]. Future studies will examine how architecture could regulate BMP4 expression. We note that our lumens cultured in pure Matrigel 3D culture were able to maintain their pluripotency for 7 days whereas some studies observed some spontaneous differentiation of stem cells cultured in Matrigel after only 3-5 days of culture [41,52]. This difference could be explained by iPSC cell line specific differences which should be further explored.

A major goal of the tissue engineering field is to synthesize biomaterials which mimic tissue level structure [53,54]. In this study, we developed collagen island hydrogels which capture the heterogeneous mesoscopic features seen in tissue. The bulk mechanical properties and mesoscopic feature size of these gels can be tuned to study cell behavior in a variety of physiologically relevant environments. These island architectures act as bioactive cues, and we found that these island gels can modulate stem cell behavior. Though globally soft materials, these gels are able to induce osteogenic commitment as well as mesodermal differentiation. These island gels can be precisely controlled and incorporated with a number of cell types and co-gel biomaterials to induce cellular self-assembly processes, including microtissue fabrication and tissue morphogenesis. These island gels have the potential in the tissue engineering space to not only understand the interactions between stem cells and physical cues but also to direct differentiation for regenerative medicine applications.

Materials and Methods

SHG Imaging

HCC cases were selected from the Yale New Haven Hospital pathology database. No approval from a research ethics committee was required for this study, as coded tissue obtained from routine diagnostic workflow was used and the included patients are not affected by the study. Anonymous or coded use of redundant tissue for research purposes is part of the standard treatment agreement with patients, to which patients may opt out. None of the included patients submitted an objection against use of residual material.

Antigen retrieval and slide staining for SHG imaging were adapted from previous protocols . Formalin fixed slides were first incubated at 55 for 10 minutes. Slides were then immersed in Xylene baths 2 times, for 5 minutes each time, to wash off paraffin. Slides were then immersed in a series of ethanol baths to rehydrate tissue. Slides were then soaked in DI water to hydrate. Tissues were then immersed in 10mM Sodium Citrate, 0.05% Tween 20, pH 6 solution at 95C for 15 minutes. The solution was then brought down to room temperature, and slides were removed and carefully dried. The sample was then outlined

with a hydrophobic pen. The sample was then soaked in TBS+0.025% TritonX-100 two times for 5 minutes each. The tissue was then blocked in TBS+10% BSA at RT for 2 hours. Tissue samples were then stained with DAPI for 1 hour at room temperature. Samples were mounted in Vectashield before imaging.

Images were acquired using two-photon microscopy (MaiTai Ti:Sapphire Laser, Spectra Physics) with a ×40 and excitation at 890 and 1,090 nm.

COMSOL Simulations

Flow simulations corresponding to the pipetting cycles were performed in Comsol Multiphysics. The computational domain was originally limited to the pipette tip, however we suspected that interactions between the flow and the microcentrifuge tube would be significant, thus we expanded the domain to include the fluid both inside the micropipette tip and the microcentrifuge tube. The geometry of the P200 micropipette (Thermo Scientific ART) and the 1.5mL microcentrifuge tube (USA Scientific) were built in Comsol Multiphysics as an axisymmetric model. The model was meshed using the adaptive mesh refinement tool within the Time-Dependent Solver to obtain a grid of 5716 triangular elements and 438 edge elements. The effects of Col. I crosslinking and other chemical reactions were ignored, so the properties of the fluid domain were simplified as water at 303.15 K. To simulate the cycle of pipetting in and pipetting out at different frequencies, the inlet boundary condition of the Laminar Flow study was defined by overlapping two functions: a positive mass flow rate (m') times a step function going from 0 to T seconds, and a negative mass flow rate (-m') times a step function from T to 2T seconds. Periods (T) of 2, 5 and 10 seconds were defined in a Parametric Sweep study. To reduce computational time, a single cycle of flow out-in was simulated for each condition. Thus, the time length of each Time Dependent study was set at 2T (0.1sec steps) and solved using the PARDISO Direct Solver. Using the solution for shear rate ($\dot{\gamma}$), we computed the shear stress ($\boldsymbol{\tau}$) for each element through the geometry using for each element through the geometry using $\tau = \mu\dot{\gamma}$, where μ is the viscosity of the fluid. The computed shear stress was then integrated over the volume of the geometry V to obtain the instantaneous shearing energy for each time step n:

$$\varepsilon[n] = \int_V \tau[n] dV$$

which is the average energy between two consecutive timepoints. Therefore, for any length of time T, we can compute the total shearing energy delivered to the fluid as

$$\varepsilon[T] = \sum_{n=0}^{T} \frac{\varepsilon[n]}{N}$$

Where N is the total number of time steps between times 0 and T.

Rheometry

An Anton Parr Shear Stress Rheometer (502 WESP) was used for mechanical characterization of collagen gels with the 25-mm parallel-plate geometry and a 500μm gap.

A no. 1 25-mm cover glass (VWR) was used for the top plate and a 40 mm cover glass (Fisherbrand) as the bottom plate. To prevent slip between the gel and the plate, both plates were chemically treated with polydopamine and attached to each plate of the rheometer with double-sided tape (3M 666). The rheometer was then zeroed and calibrated. The temperature of the system is preset and maintained at 37°C. Collagen was deposited onto the bottom plate of the rheometer immediately before gelation, and the top plate was lowered rapidly so that the gel formed a uniform disk between the two plates. Approximately 350 μL collagen was pipetted onto the rheometer, the gap was set to 500μm, and the sample was kept in a custom made humidity chamber to prevent evaporation. Polymerization progress was monitored by imposing three cycles of 0.5% strain every 5 min, measuring the shear storage modulus G' as a function of polymerization time. After at least 60 minutes of gelation, gels were immersed in PBS and allowed to sit for at least 15 minutes before taking measurements. For strain sweep measurements, collagen gels were subjected to 5 oscillations at 0.1 Hz at increasing amplitudes from 2 to 12% in 2% increments and 12 to 100% in 4% increments. Custom Python scripts were used to determine the differential shear moduli and subsequent metrics. For stress relaxation measurements, strains were applied with a rise time of 0.15 s. Only one stress relaxation test is conducted on any given sample. Custom Python scripts were used to determine the relaxation moduli, peak stress, and half max relaxation time (τ).

Cell Culture

D1 MSC cells were obtained from the American Type Culture Collection (ATCC; Manassas, VA, USA). ATCC validated all cell lines by Short Tandem Repeat Analysis. Cells were maintained at 37 °C, 5% CO2. D1 MSCs were maintained in Dulbecco's Modified Eagle's Medium (DMEM) medium supplemented with 10% fetal bovine serum, 1% L-glutamine, and 1% penicillin/streptomycin. Media was changed every other day, and cells were split every 3-4 days. To generate MSC cells expressing LifeAct–GFP, lentiviral particles containing a pLentiCMV-MCS-LifeAct-GFP vector were used. Cells were selected with puromycin (10 μg ml−1). They are cultured at no more than 80% confluency at no greater than passage 25 in serum-supplemented DMEM.

The hiPSCs were a gift from Dr. Stuart Campbell (Department of Biomedical Engineering, Yale University). hiPSCs were cultured on TC-treated 6-well plates (Costar, Corning) coated with lactose dehydrogenase elevating virus (LDEV)-free human-embryonic-stem-cell-qualified Matrigel (Corning, 354277) in mTeSR1 media (STEMCELL Technologies) at 37 °C in 5% CO2. Media was changed daily. hiPSCs cultured in mTeSR1 were passaged at 70% confluency as pluripotent aggregates with manual selection using ReLeSR (STEMCELL Technologies) following the manufacturer's protocol.

Collagen gel

Each collagen gel was made by adding sufficient 0.5 N NaOH to neutralize a mixture of double-distilled H2O, 10× PBS, and acetic-acid-solubilized type I rat tail collagen (Corning, Corning, NY, USA) on ice for a final collagen concentration of 2 mg/ml. Island gels were made by first neutralizing 350ul of collagen. Stained collagen gels were made by incorporating 10% 647-ester dye (ThermoFisher) stained collagen. The gels were then

allowed to sit at room temperature for 6.5 minutes. Finally, the gels were sheared with a p200 pipette tip set to 175ul at a specified frequency for 3 minutes before being plated. Prior to depositing the collagen, plates used for collagen gel seeding were surface-coated with polydopamine, as previously described [37,38,55]. This coating allows collagen gels to stick to the surface of the plates and prevents detachment of the gel. After plating, gels were transferred to an incubator at 37 °C with 5% CO2 for 1 hour.

Encapsulation of iPSCs within hydrogels

hiPSCs at 70% confluency or less were passaged as single cells using Accutase (STEMCELL Technologies), washed in mTeSR1 media, and resuspended as a single-cell suspension in mTeSR1 media with 10 × 10−6 m ROCK inhibitor (Y-27632, STEMCELL Technologies) to prevent dissociation-induced apoptosis. For 50% collagen gels, isotropic or island gels were made and mixed in equal parts on ice with Matrigel (Corning, 354277). For 20% matrigel: collagen gels, isotropic or island gels were made and mixed with Matrigel and PBS on ice such that the resulting gel was 20% Matrigel by volume. Collagen gels were made, and an appropriate amount of cells were mixed to achieve a final concentration of 100000 cells/ml. After gelation, mTeSR1 media with 10 × 10−6 m ROCK inhibitor was added. 24 h post encapsulation, the media was changed to mTeSR1 which was replenished daily.

Encapsulation of MSCs within hydrogels

D1 MSCs or D1 MSC-LifeActRFP cells were mixed with the collagen solution prior to gelation to achieve a final cell concentration of 15000 cells/ml. Cells were cultured in 50%/50% mixture of the osteogenic induction medium and adipogenic induction medium (differentiation medium). The differentiation medium contained 50 μg/ml L-ascorbic acid (MilliporeSigma), 10 mM β-glycerophosphate (MilliporeSigma), and 0.1 μM dexamethasone (MilliporeSigma) in the DMEM growth medium.

MSC time lapses were performed in 12 well glass bottom dishes which had been polydopamine coated. 12 hour time lapses were taken on Day 1 and Day 6. Automatic cell segmentation was obtained using Imaris (Oxford Instruments). Manual filtering was done to determine which cells were to be used for downstream analysis. From these segmentations, cell movement was tracked and metrics such as mean speed, sphericity, and migration track length over the timelapse were obtained. Mean speed is defined as the average of instantaneous speeds between timepoints.

MSD Image Analysis

Custom Python3 scripts were used to calculate MSD plots. Trajectories were exported to Python to calculate average speed and mean squared displacement. Average speed specifically refers to the mean of the absolute value of the net displacement of the cell center per hour. Mean squared displacements $MSD(n)$ were computed with the following equation [56]:

$$MSD(n) = \frac{1}{(N-n+1)} \sum_{i=0}^{N-n} \left[(x_{i+n} - x_i)^2 + (y_{i+n} - y_i)^2 + (z_{i+n} - z_i)^2 \right]$$

where N is the total number of steps, n is the n-th step, and x,y,z are the x,y,z coordinates, respectively.

Gel Compaction

Gel compaction experiments were performed in 24 well plastic bottom plates. Wells were incubated with 3% BSA for 1 hour and then washed with PBS to avoid adhesion of the gel to the plate. D1 MSCs were mixed with 500 μL of collagen solution prior to gelation to achieve a final cell concentration of 600000 cells/ml. Cells were cultured in the differentiation medium described above, and media was changed everyday. Images of the gels were taken everyday for 7 days. After 7 days of culture, gels were treated with an 8% Triton and 0.125% Trypsin-EDTA solution for 30 minutes to decellularize our gels and observe the degree of plastic deformation. Images of the gels were taken after decellularization.

Timelapses of gel compaction assays were performed in 15 well plates (Ibidi). Cells were incubated with 3% BSA for 1 hour and then washed with PBS to avoid adhesion of the gel to the plate. D1 MSCs were mixed with 15 μL of collagen solution prior to gelation to achieve a final cell concentration of 600000 cells/ml. Cells were cultured in 50 μL of the differentiation medium described above. Images were taken every 6 minutes for 12 hours.

Confocal microscopy

A Leica SP8 laser scanning confocal microscope with a ×10 objective or × 5 objective (Wetzlar, Germany) was used for live imaging of MSC's. The 10x objective was used for 7 day time lapse experiments, and Z-stacks were taken with a thickness of 2um. 12 hour time lapses were taken on Day 1 and Day 6. The 10x was used for 12 hour gel compaction experiments, and Z-stacks were taken with a thickness of 5um. A temperature of 37 °C and a 5% CO2 atmosphere were maintained using a humidified OKO labs live-cell imaging incubator. 3D fluorescence images were taken with either a 20x objective or 40x water objective. 3D Z stacks were taken with a thickness of 2um. Cell and nuclear outlines were manually traced in ImageJ.

Island architectures/pore size were segmented from 20x images. In ImageJ, islands were thresholded and segmented in order to achieve metrics for island size. Line intensity profiles were also obtained from each island architecture with ImageJ to determine island distribution. Custom Python scripts were then used to perform Fourier analysis on these line intensity profiles.

Scanning Electron Microscopy

The collagen sample is placed in 4% paraformaldehyde (Thermo Fisher Scientific) for 1hour at room temperature. We then soak the sample twice in PBS for 10 minutes each. This is followed by two 10 minute ddH2O washes. We then put the sample through a graded

ethanol + H2O wash for 10 minutes each in this order: 30% EtOH, 50% EtOH, 66% EtOH, and 100% EtOH. We then put the sample through a graded ethanol + HMDS wash for 10 minutes each in this order: 30% HMDS, 50% HMDS, 66% HMDS, and 100% HMDS. Samples were then placed on aluminum foil and allowed to dry in the fume hood overnight. Subsequently, the samples were mounted on a support with carbon tape and covered with a 8 nm layer of iridium with a sputter coater. The samples were then imaged with a scanning electron microscope.

Immunofluorescence staining

Gels were rinsed twice with PBS and fixed with 4% paraformaldehyde (Thermo Fisher Scientific) in PBS for 25 min at room temperature. Following fixation, gels were permeabilized with 0.2% Triton X-100 in PBS for 1 h at room temperature. They were then blocked with 3% BSA in PBS containing 0.01% Triton X-100 for 3 h at room temperature. The samples were then incubated for 24 h at 4 °C with the primary antibody Nanog (1:100; α-Rabbit; Cell Signaling Technologies), SOX2 (1:100; α-Rabbit; Cell Signaling Technologies), Oct4 (1:200; α-Rabbit; Cell Signaling Technologies), Vimentin (1:200; α-mouse; Santa Cruz), SNAIL (1:200; α-Goat; R&D Systems), Brachyury (1:100; α-Goat; R&D Systems), or RUNX2 (1:100; Mouse; Cell Signaling Technologies). After washing for 3-5 h at room temperature, samples were incubated overnight at 4 °C with secondary antibody Alexa 647 goat-α-rabbit (1:1000 in PBS; Invitrogen), Alexa Fluor donkey-α-goat (1:1000 in PBS; Invitrogen), or Alexa 488 goat-α-mouse (1:1000 in PBS; Invitrogen), DAPI (1:2,000, Invitrogen) and phalloidin-Alexa 555 (1:500; Abcam). After at least 3 hours of washing, samples were mounted in Vectashield (Vector Laboratories) before imaging.

mRNA quantitative testing

To quantify stem cell differentiation, mRNA from iPSCs cultured in gels for 7 days were extracted. At least 3 gels per replicate were suspended in Trizol and homogenized with a 20G needle. RNA was isolated by phenol–chloroform extraction and subsequent RNA extraction columns from the RNEasy Extraction Kit (Qiagen). 5 μg of RNA were reverse transcribed and amplified using the iTaq Universal SYBR Green One Step Kit (BioRad). Samples were analyzed using the Bio-Rad iTaq Universal Probes One-Step Kit in 20-μl reactions run at 50 °C for 10 min and 95 °C for 1 min, followed by 40 cycles of 95 °C for 10 s and 60 °C for 2 minutes per the manufacturer's recommendations. Primers are reported in Supplementary Table 1. Reactions were performed on an Applied Biosystems 7500 instrument.

Differentiation staining

ALP was stained with a FastBlue working solution of 500 μg/ml Fast Blue BB (MilliporeSigma) and 500 μg/ml naphthol-AS-MX (MilliporeSigma) phosphate in an alkaline buffer (100 mM Tris-HCl, 100 mM NaCl, 0.1% Tween-20, 50 mM MgCl2, pH = 8.2). Fixed samples were first washed three times in DPBS, equilibrated in alkaline buffer for 15 min, then incubated in FastBlue working solution for 60 min at room temperature. The samples were then washed in alkaline buffer for 15 min followed by 15 min in DPBS. For Oil Red staining, gels were equilibrated with 60% isopropanol for 30 minutes before being incubated in Oil Red in 60% isopropanol for 1 hour. Gels were then washed three

times with H2O for 1 hour before imaging. For Alizarin Red staining, fixed samples were first equilibrated with water for 30 minutes. Gels were then incubated in 2% ARS solution (Sigma) for 30 minutes. Gels were then washed three times with H2O for an hour. Samples were then imaged after 7 days on a Leica DMI1 transmitted light microscope.

Statistics and reproducibility

GraphPad Prism was used for all statistical analyses. *In vitro* experiments were repeated at least three independent times. To compare differences between more than two groups, a one-way ANOVA with Tukey's post-hoc test was used. Different levels of statistical significance were set at $*p < 0.05$, $**p < 0.01$, $***p < 0.001$, $****p < 0.0001$.

Automatic Collagen Mixer

In order to further validate the replicability of the unique Collagen I architecture, a computer-controlled extruder was designed and constructed. Conventional off the shelf syringe pumps offer the accuracy required for this application; however, they tend to be heavy, bulky, costly and few offer the option of running custom pumping sequences without bypassing the whole controller board and connecting directly to the motor. It was therefore decided that to achieve the desired pumping in/out cycle, the best option would be to design a linear actuator that could operate any syringe and would be light enough to attach to a scaffold over the hot plate. The main components of the actuator are: a 3D-printed frame, a Nema 17 stepper motor, a A4988 stepper driver, a set of 20T/60T GT2 gears, a T8 2mm pitch lead screw, and an Arduino Uno microcontroller. The complete structure was printed in 11h using an Elegoo Saturn resin printer. The Arduino IDE was used to program and upload the code on the board. Using the known gear ratios and rotational-to-linear motion conversion of the lead screw, we adjusted the speed of the stepper motor to obtain the desired flow rates. The complete Collagen shearing system can be built for less than $200.

Supplementary Material

Refer to Web version on PubMed Central for supplementary material.

Acknowledgments

R.Y.N. was supported by NIH grant T32EB019941. We acknowledge support from the National Institutes of Health National Institute of General Medical Sciences grant number R35GM142875 to M.M. We thank Hugh Xiao for technical assistance with the gel compaction studies.

Data Availability

All data supporting the results in this study are available within the Article and its Supplementary Information. Manuscript raw data and data points can be found at (https://figshare.com/s/e20de08b75ba42fd21d4). All other data are available from the corresponding author upon reasonable request.

References

1. Boraschi-Diaz I, Wang J, Mort JS & Komarova SV Collagen Type I as a Ligand for Receptor-Mediated Signaling. Frontiers in Physics vol. 5 Preprint at 10.3389/fphy.2017.00012 (2017).

2. Dupont S et al. Role of YAP/TAZ in mechanotransduction. Nature 474, 179–183 (2011). [PubMed: 21654799]
3. Paszek MJ et al. Tensional homeostasis and the malignant phenotype. Cancer Cell 8, 241–254 (2005). [PubMed: 16169468]
4. Wong SW, Lenzini S, Cooper MH, Mooney DJ & Shin J-W Soft extracellular matrix enhances inflammatory activation of mesenchymal stromal cells to induce monocyte production and trafficking. Sci Adv 6, eaaw0158 (2020). [PubMed: 32284989]
5. Motte S & Kaufman LJ Strain stiffening in collagen I networks. Biopolymers 99, 35–46 (2013). [PubMed: 23097228]
6. Shellard A & Mayor R Collective durotaxis along a self-generated stiffness gradient in vivo. Nature 600, 690–694 (2021). [PubMed: 34880503]
7. Huebsch N et al. Harnessing traction-mediated manipulation of the cell/matrix interface to control stem-cell fate. Nat. Mater 9, 518–526 (2010). [PubMed: 20418863]
8. Conklin MW et al. Aligned collagen is a prognostic signature for survival in human breast carcinoma. Am. J. Pathol 178, 1221–1232 (2011). [PubMed: 21356373]
9. Barriga EH, Franze K, Charras G & Mayor R Tissue stiffening coordinates morphogenesis by triggering collective cell migration in vivo. Nature 554, 523–527 (2018). [PubMed: 29443958]
10. Engler AJ, Sen S & Discher DE Matrix elasticity directs stem cell differentiation. Journal of Biomechanics vol. 39 S269 Preprint at 10.1016/s0021-9290(06)84031-5 (2006).
11. Vader D, Kabla A, Weitz D & Mahadevan L Strain-Induced Alignment in Collagen Gels. PLoS One 4, (2009).
12. Münster S et al. Strain history dependence of the nonlinear stress response of fibrin and collagen networks. Proc. Natl. Acad. Sci. U. S. A 110, 12197–12202 (2013). [PubMed: 23754380]
13. Malandrino A, Trepat X, Kamm RD & Mak M Dynamic filopodial forces induce accumulation, damage, and plastic remodeling of 3D extracellular matrices. PLoS Comput. Biol 15, e1006684 (2019). [PubMed: 30958816]
14. 3D mesenchymal cell migration is driven by anterior cellular contraction that generates an extracellular matrix prestrain. Dev. Cell 56, 826–841.e4 (2021). [PubMed: 33705692]
15. Hall MS et al. Fibrous nonlinear elasticity enables positive mechanical feedback between cells and ECMs. Proc. Natl. Acad. Sci. U. S. A 113, 14043–14048 (2016). [PubMed: 27872289]
16. Davidson MD et al. Programmable and contractile materials through cell encapsulation in fibrous hydrogel assemblies. Sci Adv 7, eabi8157 (2021). [PubMed: 34757787]
17. Gong X, Kulwatno J & Mills KL Rapid fabrication of collagen bundles mimicking tumor-associated collagen architectures. Acta Biomater. 108, (2020).
18. Nerger BA, Brun P-T & Nelson CM Marangoni flows drive the alignment of fibrillar cell-laden hydrogels. Sci Adv 6, eaaz7748 (2020). [PubMed: 32582851]
19. Ahmed A et al. Local extensional flows promote long-range fiber alignment in 3D collagen hydrogels. Biofabrication 14, 035019 (2022).
20. Nerger BA, Brun P-T & Nelson CM Microextrusion printing cell-laden networks of type I collagen with patterned fiber alignment and geometry. Soft Matter 15, 5728–5738 (2019). [PubMed: 31267114]
21. Oria R et al. Force loading explains spatial sensing of ligands by cells. Nature 552, 219–224 (2017). [PubMed: 29211717]
22. Seo BR et al. Collagen microarchitecture mechanically controls myofibroblast differentiation. Proc. Natl. Acad. Sci. U. S. A 117, 11387–11398 (2020). [PubMed: 32385149]
23. Velez DO et al. 3D collagen architecture induces a conserved migratory and transcriptional response linked to vasculogenic mimicry. Nat. Commun 8, 1651 (2017). [PubMed: 29162797]
24. Winer JP, Oake S & Janmey PA Non-Linear Elasticity of Extracellular Matrices Enables Contractile Cells to Communicate Local Position and Orientation. PLoS One 4, e6382 (2009). [PubMed: 19629190]
25. Wang H, Abhilash AS, Chen CS, Wells RG & Shenoy VB Long-range force transmission in fibrous matrices enabled by tension-driven alignment of fibers. Biophys. J 107, 2592–2603 (2014). [PubMed: 25468338]

26. Rudnicki MS et al. Nonlinear Strain Stiffening Is Not Sufficient to Explain How Far Cells Can Feel on Fibrous Protein Gels. Biophysical Journal vol. 105 11–20 Preprint at 10.1016/j.bpj.2013.05.032 (2013). [PubMed: 23823219]
27. Lee H-P et al. The nuclear piston activates mechanosensitive ion channels to generate cell migration paths in confining microenvironments. Sci Adv 7, (2021).
28. Lee H-P, Gu L, Mooney DJ, Levenston ME & Chaudhuri O Mechanical confinement regulates cartilage matrix formation by chondrocytes. Nat. Mater 16, 1243–1251 (2017). [PubMed: 28967913]
29. Chaudhuri O et al. Hydrogels with tunable stress relaxation regulate stem cell fate and activity. Nat. Mater 15, 326–334 (2016). [PubMed: 26618884]
30. Chrisnandy A, Blondel D, Rezakhani S, Broguiere N & Lutolf MP Synthetic dynamic hydrogels promote degradation-independent in vitro organogenesis. Nat. Mater 21, 479–487 (2022). [PubMed: 34782747]
31. Nam S, Hu KH, Butte MJ & Chaudhuri O Strain-enhanced stress relaxation impacts nonlinear elasticity in collagen gels. Proc. Natl. Acad. Sci. U. S. A 113, 5492–5497 (2016). [PubMed: 27140623]
32. Bordeleau F et al. Matrix stiffening promotes a tumor vasculature phenotype. Proc. Natl. Acad. Sci. U. S. A 114, 492–497 (2017). [PubMed: 28034921]
33. Han YL et al. Cell contraction induces long-ranged stress stiffening in the extracellular matrix. Proc. Natl. Acad. Sci. U. S. A 115, 4075–4080 (2018). [PubMed: 29618614]
34. Janmey PA, Fletcher DA & Reinhart-King CA Stiffness Sensing by Cells. Physiol. Rev 100, 695 (2020). [PubMed: 31751165]
35. Ghibaudo M et al. Traction forces and rigidity sensing regulate cell functions. Soft Matter 4, 1836–1843 (2008).
36. Carey SP et al. Local extracellular matrix alignment directs cellular protrusion dynamics and migration through Rac1 and FAK. Int Bio (Cam) 8, 821–835 (2016).
37. Nguyen RY et al. Cytoskeletal dynamics regulates stromal invasion behavior of distinct liver cancer subtypes. Communications Biology vol. 5 Preprint at 10.1038/s42003-022-03121-5 (2022).
38. Park SE, Georgescu A, Oh JM, Kwon KW & Huh D Polydopamine-Based Interfacial Engineering of Extracellular Matrix Hydrogels for the Construction and Long-Term Maintenance of Living Three-Dimensional Tissues. ACS Appl. Mater. Interfaces 11, 23919–23925 (2019). [PubMed: 31199616]
39. Zhao Z, Zhao M, Xiao G & Franceschi RT Gene transfer of the Runx2 transcription factor enhances osteogenic activity of bone marrow stromal cells in vitro and in vivo. Mol. Ther. 12, 247–253 (2005). [PubMed: 16043096]
40. Yang C, Tibbitt MW, Basta L & Anseth KS Mechanical memory and dosing influence stem cell fate. Nat. Mater 13, 645–652 (2014). [PubMed: 24633344]
41. Simunovic M et al. A 3D model of a human epiblast reveals BMP4-driven symmetry breaking. Nat. Cell Biol 21, 900–910 (2019). [PubMed: 31263269]
42. Lumen Formation Is an Intrinsic Property of Isolated Human Pluripotent Stem Cells. Stem Cell Reports 5, 954–962 (2015). [PubMed: 26626176]
43. Carver EA, Jiang R, Lan Y, Oram KF & Gridley T The Mouse Snail Gene Encodes a Key Regulator of the Epithelial-Mesenchymal Transition. Mol. Cell. Biol 21, 8184 (2001). [PubMed: 11689706]
44. Provenzano PP et al. Collagen reorganization at the tumor-stromal interface facilitates local invasion. BMC Med. 4, 38 (2006). [PubMed: 17190588]
45. Cicchi R et al. Scoring of collagen organization in healthy and diseased human dermis by multiphoton microscopy. J. Biophotonics 3, 34–43 (2010). [PubMed: 19771581]
46. Caiazzo M et al. Defined three-dimensional microenvironments boost induction of pluripotency. Nat. Mater 15, 344–352 (2016). [PubMed: 26752655]
47. Navarro RS et al. Tuning Polymer Hydrophilicity to Regulate Gel Mechanics and Encapsulated Cell Morphology. Adv. Healthc. Mater 11, e2200011 (2022). [PubMed: 35373510]

48. Mak M, Zaman MH, Kamm RD & Kim T Interplay of active processes modulates tension and drives phase transition in self-renewing, motor-driven cytoskeletal networks. Nat. Commun 7, 10323 (2016). [PubMed: 26744226]

49. Impact of crosslink heterogeneity on extracellular matrix mechanics and remodeling. Comput. Struct. Biotechnol. J 18, 3969–3976 (2020). [PubMed: 33335693]

50. Zheng Y et al. Controlled modelling of human epiblast and amnion development using stem cells. Nature 573, 421–425 (2019). [PubMed: 31511693]

51. Zhang P et al. Short-term BMP-4 treatment initiates mesoderm induction in human embryonic stem cells. Blood 111, 1933–1941 (2008). [PubMed: 18042803]

52. Indana D, Agarwal P, Bhutani N & Chaudhuri O Viscoelasticity and Adhesion Signaling in Biomaterials Control Human Pluripotent Stem Cell Morphogenesis in 3D Culture. Adv. Mater 33, e2101966 (2021). [PubMed: 34499389]

53. Molley TG, Hung T & Kilian KA Cell-laden Gradient Microgel Suspensions for Spatial Control of Differentiation During Biofabrication. Advanced Healthcare Materials 2201122 Preprint at 10.1002/adhm.202201122 (2022).

54. Daly AC, Riley L, Segura T & Burdick JA Hydrogel microparticles for biomedical applications. Nature reviews. Materials 5, (2020).

55. Lee H, Dellatore SM, Miller WM & Messersmith PB Mussel-inspired surface chemistry for multifunctional coatings. Science 318, 426–430 (2007). [PubMed: 17947576]

56. Gorelik R & Gautreau A Quantitative and unbiased analysis of directional persistence in cell migration. Nat. Protoc 9, 1931–1943 (2014). [PubMed: 25033209]

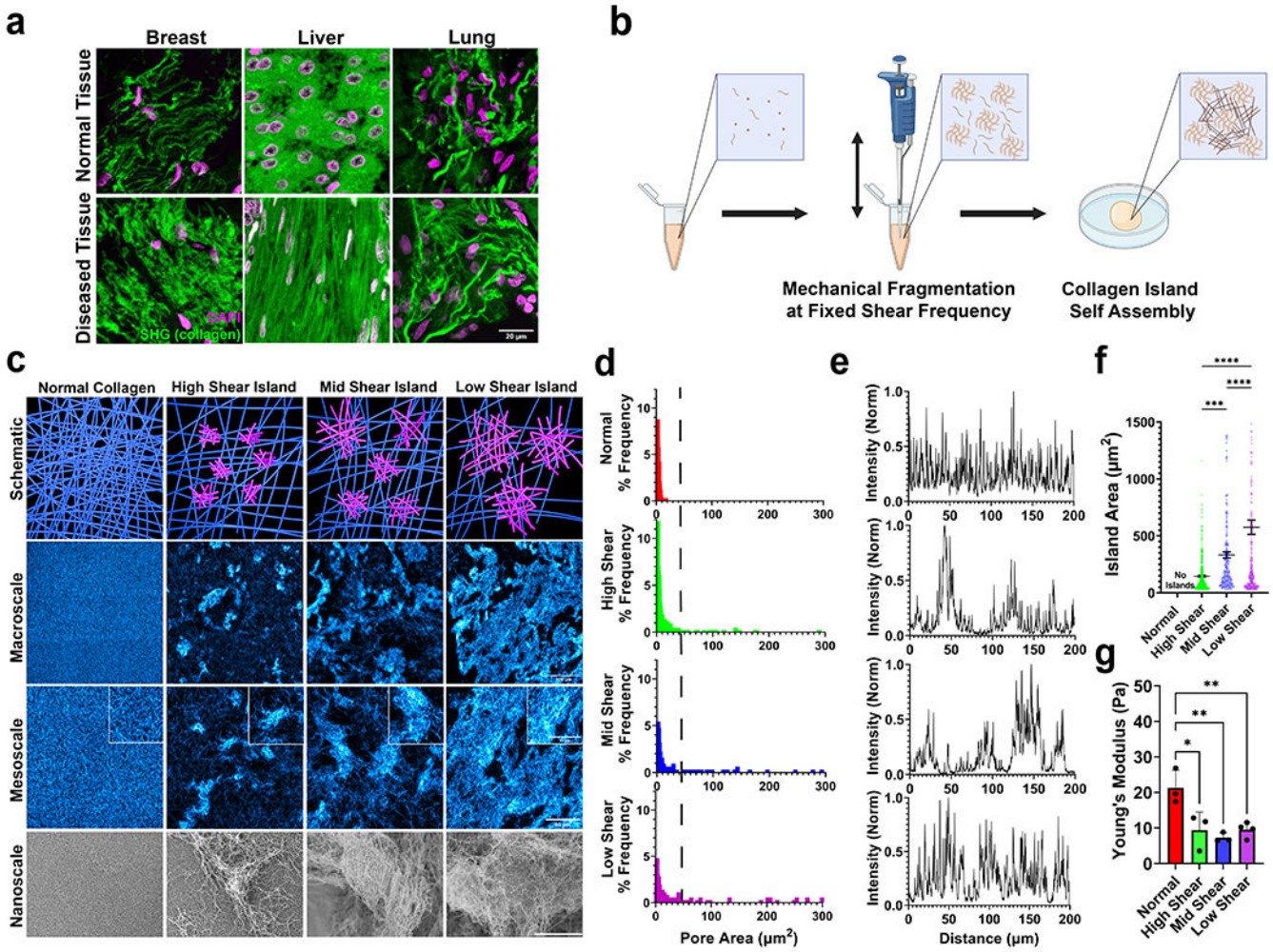

Figure 1 - Tunable Collagen Island architectures mimic tissue topology.

(a) Collagen architecture in tissue is diverse. Images are representative of normal (top) and diseased (bottom) breast, liver, and lung tissue. Scale bar is 20 um. (b) Schematic detailing collagen island assembly protocol. Made with Biorender.com. (c) Collagen island architecture schematic as a function of shear frequency and architecture imaged with confocal microscopy (stained collagen in cyan) and scanning electron microscopy to visualize macro, meso, and nanoscale. Scale bar in the second row is 100 μm. Scale bars in the third row and corresponding inset are 50 μm and 30 μm, respectively. Scale bar in the fourth row is 20 μm. (d) Pore area distribution for each island architecture. Right of dotted line indicates frequency of larger pore areas and therefore sparser collagen. (e) Cross sectional distribution of collagen architecture in a randomly selected location on confocal images. (f) Island area measured from confocal imaging, mean ± sem. (g) Young's modulus of island gels measured from shear rheometry. N ≥ 3 independent gels, mean ± sd. *, $p < 0.05$; **, $p < 0.01$; ***$p < 0.0001$ by one-way ANOVA.

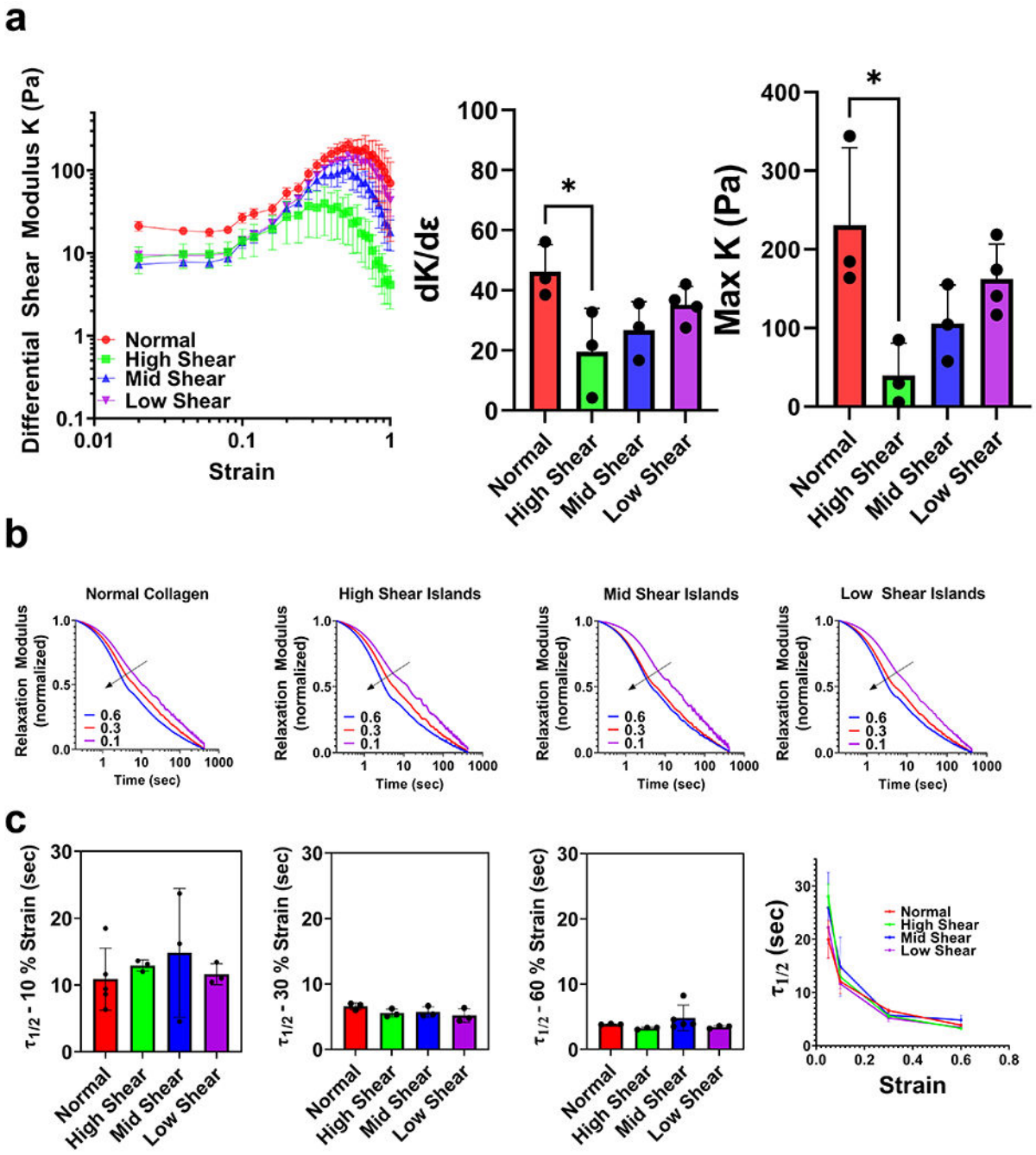

Figure 2 - Mechanical properties of collagen islands are tunable.

(a) Strain sweeps of island gels. Differential shear modulus K as function of shear strain. Corresponding rate of strain stiffening (dK/dE) and maximum shear modulus for each architecture. N ≥ 3, mean ± sem, (b) Average normalized stress relaxation tests at different strains. Blue is 60%, red is 30%, and purple is 10% strain. Black line indicates decreasing half max relaxation time as hold strain increases. (c) $\tau_{1/2}$ values for each island architecture at each given strain. While $\tau_{1/2}$ decreases with increasing strain, there is no significant

change in $\tau_{1/2}$ values as a result of island architecture introduction. N ≥ 3, mean ± sd. * $p < 0.05$ by one-way ANOVA.

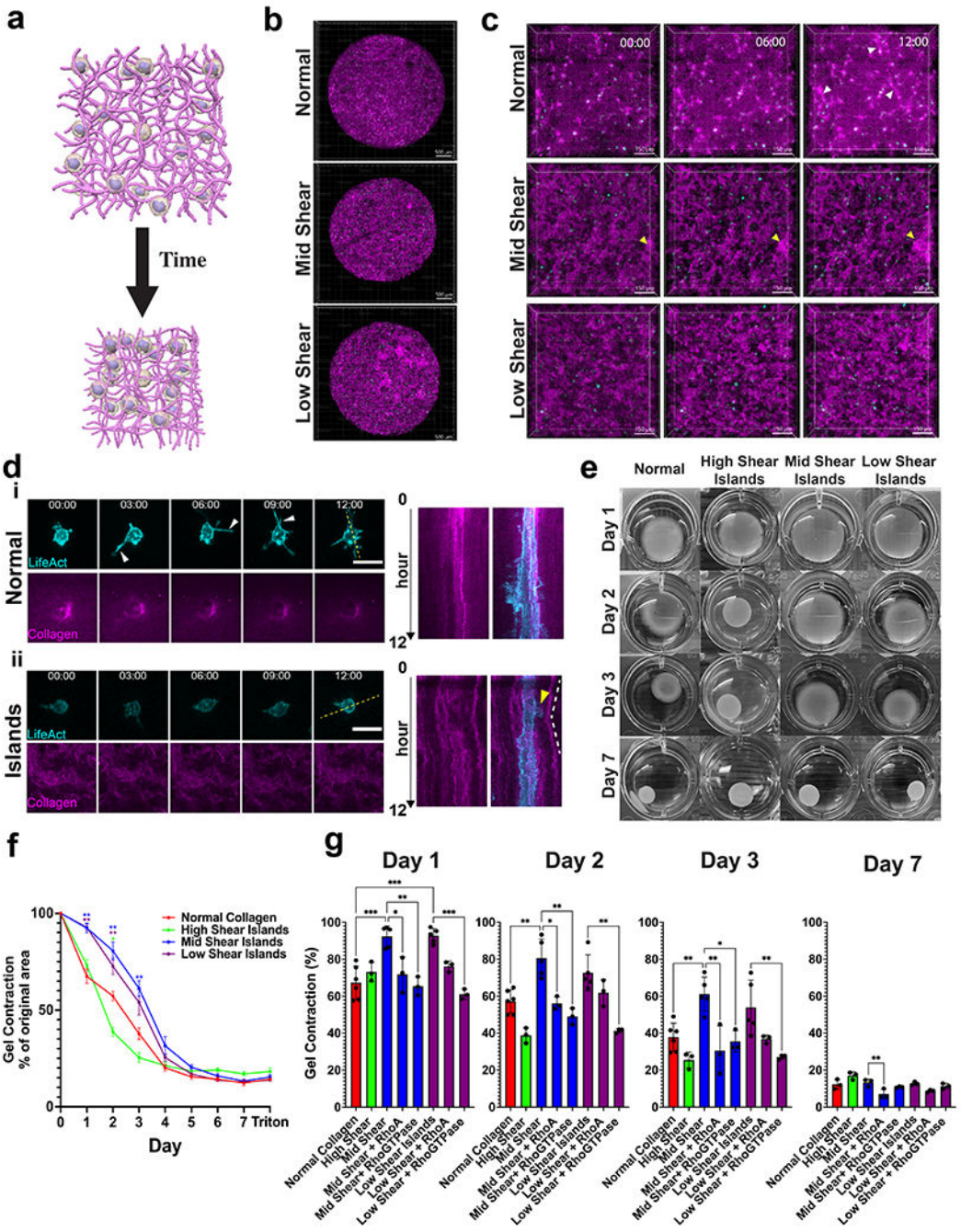

Figure 3 - Cell contractile behavior is modulated by heterogeneous architecture.

(a) Schematic of gel compaction assay. (b) Representative timelapse and (c) zoomed in images of MSCs in smaller gel volumes over 12 hours. White arrows indicate plastic gel tracks formed between cells. Yellow arrows indicate island architecture movement. Scalebar for (b) is 500 μm and for (c) is 150 μm. (d) Representative images and kymograph for MSCs cultured in (i) normal or (ii) mid shear island gels. Yellow arrow indicates dynamic protrusion and white lines indicate island architecture movement. Scale bar is 30 μm. (e) Gel compaction for MSCs (6x10^5 cells/ml) for varied island architectures over 7 days. N

≥ 3, mean ± sem. (f) 7 day time course of MSCs cultured in each island architecture . (g) Quantified gel compaction area at days 1,2,3 and 7 for each island gel. N ≥ 3, mean ± sd. Magenta is stained collagen and cyan is MSC-LifeAct cells. * $p < 0.05$; **, $p < 0.01$; ***$p < 0.0001$ by one-way ANOVA.

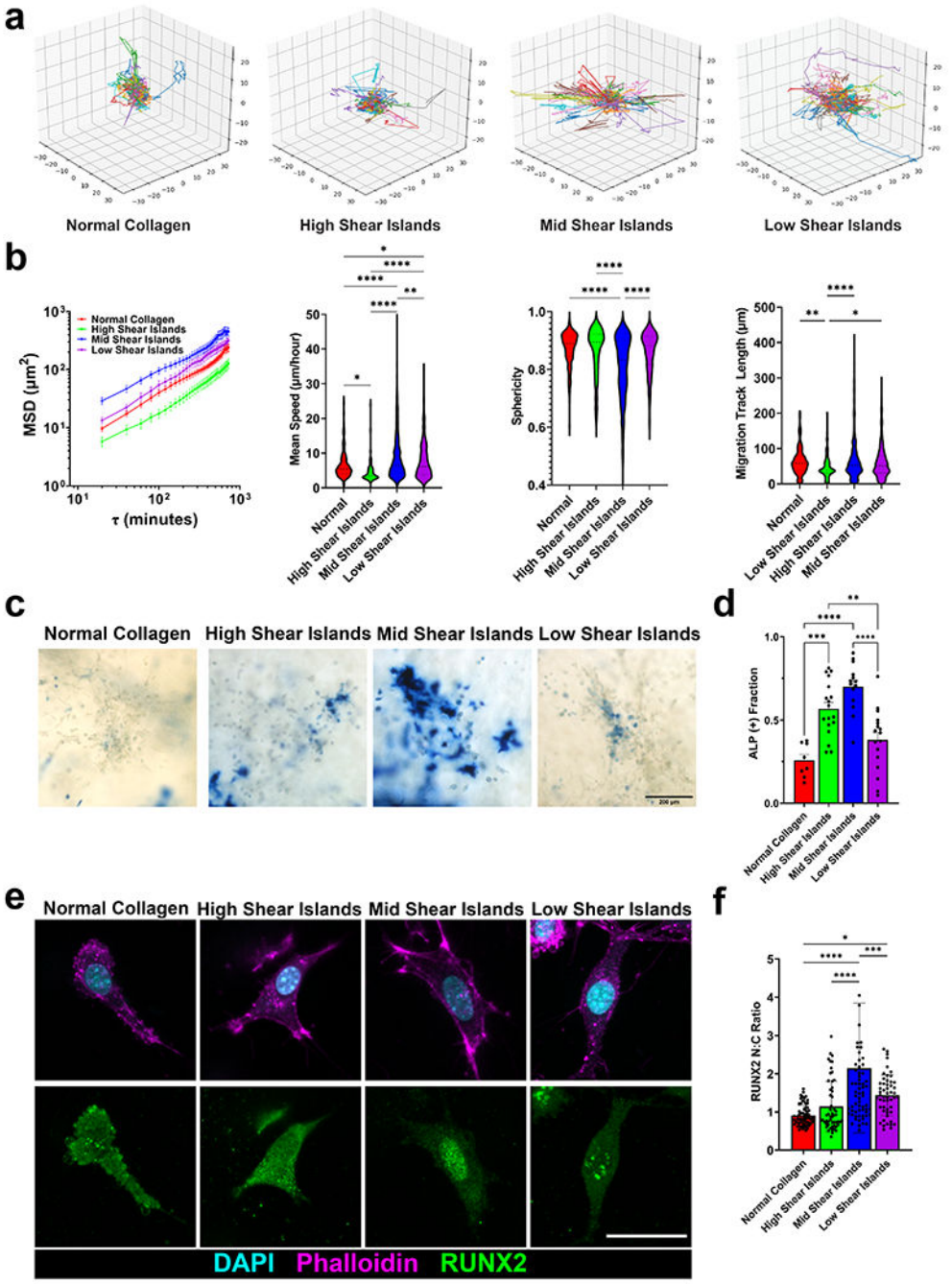

Figure 4 - MSC migratory and differentiation behaviors are modulated by island architecture.

(a) Representative 3D track reconstructions for cell migration in island architectures. (b) Mean squared displacements, mean speeds, sphericity, and migration track length for migrating cells. N = 3, n > 200 cells. (c) Representative images of alkaline phosphatase staining (blue), indicating early osteogenic differentiation, for MSC cultured in island gels for 7 days. Scale bar is 200 μm. (d) Corresponding ALP (+) fraction of cells. n ≥ 3 images from 3 independent replicates. (e) Representative images of RUNX2 (green), DAPI (cyan), and F-actin (magenta) of MSCs cultured in island gels for 7 days. (f) Corresponding

RUNX2 nuclear to cytoplasmic ratio of cells cultured in each island gel. N=3, n > 53 cells. Scale bar is 30 microns. mean ± sd * $p < 0.05$; **, $p < 0.01$; ***$p < 0.0001$ by one-way ANOVA.

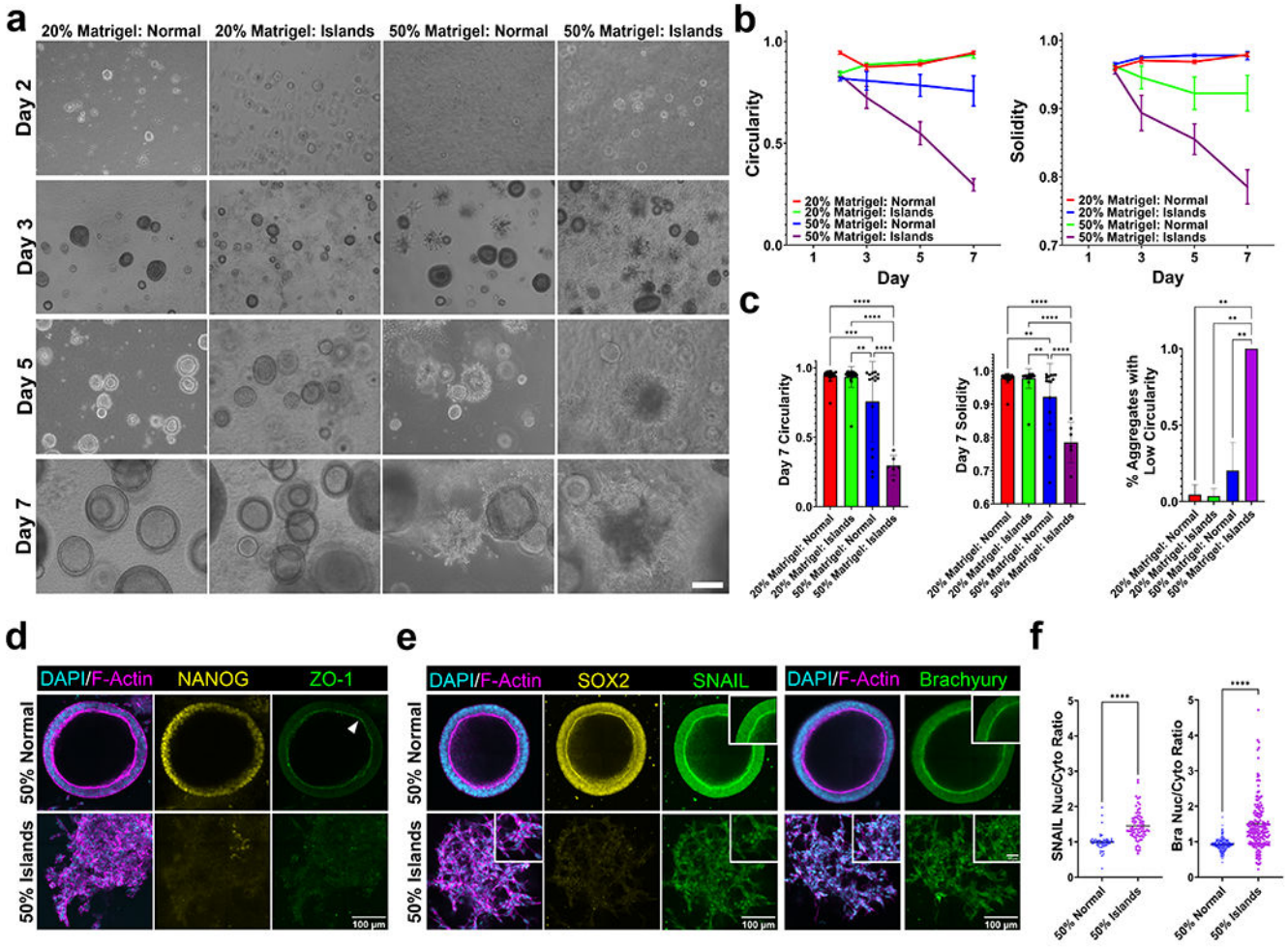

Figure 5 - iPSCs undergo mesodermal transitions in island architecture.

(a) Representative images of iPSCs grown in normal or mid shear islands in co-gels with either 20% Matrigel by volume or 50% Matrigel by volume over 7 days. Scale bar is 200 μm. (b) Circularity and solidity of iPSC aggregates over 7 days and significantly decreases in matrigel: island co-gels. (c) Quantified solidity, circularity, and % aggregates with low circularity (< 0.7) after 7 days of culture. N = 3, n > 5 aggregates, mean ± sd (d) Representative immunofluorescent images of 50% Matrigel: Normal and 50% Matrigel:Island gels stained for DAPI (cyan), F-actin (magenta), Nanog (yellow) and ZO-1 (green) after 7 days of culture. iPSCs cultured in island co-gels lose their pluripotency and apical-basal polarity indicated by loss of Nanog and ZO-1, respectively. (e) After 7 days of culture, iPSCs show mesodermal differentiation in 50% Matrigel:Island gels indicated by nuclear localization of (left) Snail and (right) Brachyury (insets). (f) Corresponding nuclear to cytoplasmic ratio of SNAIL (left) and Brachyury (right). Scale bar is 100 μm. Inset scale bar is 30 μm. mean ± sd * $p < 0.05$; **, $p < 0.01$; ***$p < 0.001$; ***$p < 0.0001$ by one-way ANOVA.